Analysis of transmitted optical spectrum enabling accelerated testing of multijunction concentrating photovoltaic designs

David C. Miller
Michael D. Kempe
Cheryl E. Kennedy
Sarah R. Kurtz
National Renewable Energy Laboratory
1617 Cole Boulevard
Golden, Colorado 80401
E-mail: david.miller@nrel.gov

Abstract. Concentrating photovoltaic (CPV) technology has recently gained interest based on its scalability and expected low levelized cost of electricity. The reliability of encapsulation materials used in CPV systems, however, is not well established. For example, the present qualification test for CPV modules includes only real-time ultraviolet (UV) exposure, i.e., methods for accelerated UV testing have not yet been developed. To better define the stress inherent to CPV systems, the UV and infrared spectra transmitted through representative optical systems were evaluated. Measurements of optical components are used to assess expected optical performance and quantify damaging optical exposure. Optical properties (transmittance, refractive index, reflectance, and absorptance) of candidate materials (including PMMA, soda-lime glass, borosilicate glass, and quartz refractors), components (including Ag- and Al-enabled reflectors), and encapsulants (including EVA, ionomer, PDMS, PPMS, polyolefin, and PVB) were identified. The activation spectrum was calculated for the representative optical systems using an assumed action spectrum to compare the expected damaging dose of UV radiation delivered to the cell encapsulation. The dose and flux analysis identifies the significance of IR relative to UV exposure for CPV systems. Because UV light is typically more highly attenuated, the UV dose within the encapsulation may not greatly exceed the unconcentrated global solar condition, but the thermal load scales nearly directly with the geometric concentration. Relative to a previous analysis for crystalline silicon cell technology, the analysis here is performed for III-V multijunction technology. Novel aspects here also include additional materials (such as TPU encapsulation) and additional components (transmission through silicone on glass lenses, antireflective coatings, and the front glass used with reflective systems, as well as reflection off of the cell). [DOI: 10.1117/1.3530092]

Subject terms: reliability; durability; accelerated testing; polymeric materials; reflective and refractive materials.

Paper 100741PR received Sep. 15, 2010; revised manuscript received Nov. 20, 2011; accepted for publication Nov. 23, 2010; published online Jan. 31, 2011.

1 Introduction

Concentrating photovoltaic (CPV) technology has recently gained interest based on its scalability and expected low levelized cost of electricity. In some locations, power production may be improved by illuminating high-efficiency multijunction cells[1,54] using concentrating optics[2] that track the sun to harvest its direct (versus global) radiation. Figure 1 compares the cross-section for a traditional flat-panel photovoltaic (FP-PV) system to those that may be present in refractive and/or reflective CPV systems. The figure represents the essential optical components present, including the PV cell, but does not include heat sinks or mechanical components (such as module walls or opto-mechanical fixtures). FP-PV, Fig. 1(a), uses a glass superstrate (such as low-iron soda-lime glass) as well as encapsulation (such as ethylene-co-vinyl acetate "EVA," 33 wt %. vinyl acetate) to isolate the cell from the environment while providing mechanical and optical coupling. Refractive CPV systems, Fig. 1(b) and 1(c), use a lens (such as a faceted Fresnel lens[3]) to focus light, where the geometric concentration, C_g, may be approximated from the ratio of the area of the lens perpendicular to the incident light to the absorbing area at the PV cell. Reflective systems use a mirror either to redistribute, Fig. 1(d), or focus, Fig. 1(e), the solar flux onto a PV cell. A simple flat front glass may be used in reflective systems to facilitate cleaning and improve durability (e.g., against hail impact). A kaleidoscope homogenizer (indicated in Fig. 1 as a transmitting component) is a secondary optic using total internal reflectance to improve flux uniformity, compensate for misalignment, provide for manufacturing tolerance, reduce chromatic aberration, and compensate for focusing errors, while also providing additional optical concentration.

The photodegradation of materials used in CPV systems is not well established relative to the desired service life of 30 years. The present qualification test for CPV modules[4] includes only real-time ultraviolet (UV) exposure. Methods for accelerated optical testing have not been formally developed because of the difficulty of simulating the service exposure to highly concentrated sunlight in a reasonable time. More

0091-3286/2011/$25.00 © 2011 SPIE

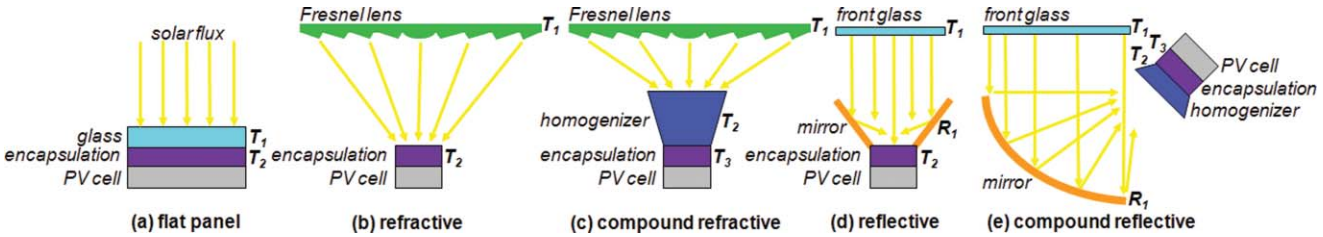

Fig. 1 Cross-sectional schematic identifying optical components present in: (a) conventional FP-PV, (b) & (c) refractive CPV, and (d) & (e) reflective CPV systems. Transmission (T_i) or reflection (R_k) events are labeled next to superstrate, lens, homogenizer, reflector, and encapsulation components.

fundamentally, the conditions inherent to the application are not widely understood. In the textile, paint, and coating industries, lifetime was historically evaluated in terms of cumulative dose of UV radiation over a broad bandwidth, such as "UV-B" (280–320 nm) or "UV-A" (320–400 nm). The variety of CPV system designs (Fig. 1), compounded with the variety of application sites, makes it very difficult to use cumulative dose as the basis for a comparative study. As popularized in the biosciences, improved correlation between field and laboratory-simulated service life is achieved if the effectiveness of the damaging radiation is considered, e.g., Eq. (1), which is based on the wavelength-specific action spectrum of the material[5,6].

$$\Lambda[\lambda] = E[\lambda]s[\lambda] = E[\lambda]c_1 e^{-c_2\lambda}. \tag{1}$$

In Eq. (1), here for system international (SI) units, Λ represents the activation spectrum $\{\mathrm{W}\cdot\mathrm{m}^{-2}\cdot\mathrm{nm}^{-1}\}$; E, the spectral irradiance $\{\mathrm{W}\cdot\mathrm{m}^{-2}\cdot\mathrm{nm}^{-1}\}$; s, the action spectrum {unitless}; and λ, the optical wavelength {nm}. As in Ref. 6, an exponential variation is assumed for the polymeric encapsulant; the coefficients $c_1 = 5.76\cdot 10^7$ {unitless} and $c_2 = 0.0697$ $\{\mathrm{nm}^{-1}\}$ are assumed here from Ref. 7. While determined in Ref. 7 for EVA specimens subject to lap shear, the choice of c_1 is somewhat arbitrary, while $c_2 = 0.0697$ may approximate hydrocarbon polymers.[8] In particular, c_2 is derived for loss of adhesion for EVA. The action spectrum indicates the sensitivity to photodegradation and is not distinguished in Eq. (1) from the quantum yield of photon interaction events.[5,6] In Eq. (1), the activation spectrum depends on the characteristics of the light source; for the variable outdoor environment this depends upon: time of day, season, specimen orientation, cloud cover, humidity, and local aerosol/ozone content. The activation spectrum is specific to the material property considered (e.g., optical transmittance, modulus, toughness) and may vary in sign at different wavelengths, e.g., being "positive" for yellowing and "negative" for the competing process of bleaching.[5,9,10] The activation spectrum can also vary according to the specimen or environment for factors including: thickness (amount of absorption), material processing (density and microstructure), material formulation (including additives, such as stabilizers), moisture concentration, temperature, and time (if damage at the surface filters transmitted light). D, the effective dose $\{\mathrm{W}\cdot\mathrm{m}^{-2}\}$, may be obtained from Eq. (2):

$$D = \int_{\lambda_i}^{\lambda_f} \Lambda[\lambda]\partial\lambda = \sum_{\lambda_i}^{\lambda_f} E[\lambda]s[\lambda]\Delta\lambda. \tag{2}$$

H, the radiant exposure $\{\mathrm{J}\cdot\mathrm{m}^{-2}\}$, is obtained from the product of dose and time, i.e., $H = Dt$.

For PV modules, the flux density of photons accounts for the energy of the light incident on the semiconductor cell and is relevant for light at or above the bandgap of the cell. If each photon is converted to an electron (100% quantum yield at the PV cell), the theoretical maximum current density identifies the electrical current that may be generated from the incoming photon flux. The theoretical maximum current density is calculated in Eq. (3).

$$\varphi = q\frac{\lambda}{hc}\phi. \tag{3}$$

Here, φ $\{\mathrm{A}\cdot\mathrm{m}^{-2}\}$ represents the theoretical maximum current density; q, the charge of a single electron $\{1.602\cdot 10^{-19}$ C$\}$; h, Planck's constant $\{6.626\cdot 10^{-34}\ \mathrm{W}\cdot\mathrm{s}^2\}$; c, the speed of light in a vacuum $\{2.998\cdot 10^8\ \mathrm{m}\cdot\mathrm{s}^{-1}\}$; and ϕ, the flux density of optical energy $\{\mathrm{W}\cdot\mathrm{m}^{-2}\}$, can be obtained from Eq. (4),

$$\phi_T = \sum_{\lambda_i}^{\lambda_f} E[\lambda]_T[\lambda]\Delta\lambda \quad \text{or} \quad \phi_R = \sum_{\lambda_i}^{\lambda_f} E[\lambda]_R[\lambda]\Delta\lambda$$

$$\text{or} \quad \phi_A = \sum_{\lambda_i}^{\lambda_f} E[\lambda]_A[\lambda]\Delta\lambda. \tag{4}$$

The subscripts T, R, and A are used in Eq. (4) to distinguish between transmitted, reflected, and absorbed quantities, respectively. The ϕ may be used for heat transfer analysis [for infrared (IR)] or quantitative comparison (for UV, often measured in units of $\mathrm{W}\cdot\mathrm{m}^{-2}$).

At this point, the operation of multijunction (MJ) cell technology should be distinguished from that of crystalline-Si (c-Si) cell technology. First, the extent of the solar spectra that may be harvested using the present III-V MJ technology extends from λ = 300–1800 nm (Ref. 1), being greater than that of c-Si, i.e., λ = 300–1120 nm. As is shown below, the greater bandwidth of operation for MJ cells ~40% greater power production from the terrestrial solar spectrum. To achieve its greater range of operation, the present MJ technology uses three junctions, each with its own unique range of operation, i.e., λ = 300–650 nm ("blue"), λ = 650–890 nm ("red"), and λ = 890–1800 nm ("IR").[1] Present MJ cells are further constrained by their electrical interconnection, i.e., the junctions are connected in series. The net harvest of energy therefore ideally occurs as the sum of the three junctions. The series connection also implies that loss occurring at one cell will affect the others; for example, a 10% loss at the blue junction will render approximately

10% power loss for the cell. In that example, secondary loss will occur via change in cell voltage.[11] The infrared junction (composed of Ge) is an exception, since it is typically overdriven;[11] therefore, unlike the blue and red junctions, the IR junction usually does not current-limit the cell and seldom compromises power production.

The goal of this study was to quantify the relative dose of damaging UV and IR radiation reaching components within a CPV module. The effective dose delivered to a polymeric encapsulant located in front of a PV cell is specifically of interest because degradation of the encapsulant material has been observed in the field for both FP-PV and CPV designs. To facilitate a fundamental understanding of light-induced degradation, the optical properties of multiple components, including lenses, homogenizers, and reflectors that might be employed in CPV were measured. The optical throughput for representative component technologies (antireflective coatings, lenses, front glass, mirrors, and cells) in the wavelengths specific to the PV application as well as UV and IR spectra were used to compare representative optical systems. The flux present in CPV systems was examined relative to FP-PV, i.e., the reference system. Because the UV and IR absorptance of representative encapsulation specimens quantifies what portions of the optical flux may contribute to degradation, a damage analysis predicting the photodegradation of a polymeric encapsulant was performed according to an assumed action spectrum. The results here, tailored to the present III-V MJ cell technology, are compared to a previous analysis for c-Si cell technology.[12] The estimates identify the stresses induced within different CPV configurations, providing insight into the operating conditions affecting system performance. The estimates here also provide a foundation for developing an accelerated-aging test methodology that may be used to evaluate candidate encapsulation materials exposed to concentrated light.

2 Experimental

Optical measurements were performed using a dual-beam ultraviolet–visible–near-infrared (UV-VIS-NIR) spectrophotometer (Lambda 900, Perkin-Elmer Inc.) with a 60-mm-diameter integrating-sphere attachment. The entrance aperture of the integrating sphere is 30 mm and its incidence angle is 8 deg. The measurement accuracy of the instrument is $\pm 0.08\%$ in the UV/VIS and $\pm 0.32\%$ in the IR, and the reproducibility is $<2 \pm 0.8\%$ (average ± 1 S.D.).[13] To adequately monitor both UV and IR performance, transmission was measured from 200–2600 nm for a 5 nm interval; likewise, reflectance was measured from 250–2500 nm, relative to a National Institute of Standards and Technology (NIST) traceable, second-surface Ag standard (and then converted to absolute reflectance). The spectra obtained according to Ref. 14 were later analyzed with the air-mass (AM) 1.5 terrestrial direct-normal solar spectrum.[15] The AM1.5 spectrum is not as intense as the AM1.05 spectrum[16] originally designed for reference relative to accelerated UV test equipment. The ASTM G177 (AM1.05) spectrum represents the maximum natural UV exposure at a challenging terrestrial application site, i.e., a sunny (desert) location high in elevation (2000 m); with low aerosol-depth (0.05 at 500 nm); low ozone content (0.30 atmosphere · centimeters); and low water vapor content (1.42 cm). The ASTM G173 (AM1.5) spectrum represents the UV exposure at a good application site, i.e., a sunny (desert) location in the southwestern USA that is low in elevation (0 m); with greater aerosol-depth (0.084 at 500 nm); greater ozone content (0.34 atm · cm); and same water vapor content (1.42 cm). All specimens (plates of glass or polymer, Fresnel lenses, encapsulants laminated between quartz slides, mirrors, and reflectors) were cleaned with a 20% vol solution of detergent (LiquiNox, Alconox Inc.) and deionized water (DI) prior to measurement.

For laminated specimens, the silica glass was buffed with pumice powder and cleaned with a detergent (Billco, Billco Manufacturing Inc.), DI, and then isopropyl alcohol prior to assembly. Polymer sheets were then assembled with a liner composed of fiberglass embedded in Poly(tetrafluoroethylene) (PTFE) to define the thickness ($\sim$0.5 mm) and cavity size. Alternately, the silicones were degassed in a vacuum chamber and then poured into a 5-mm-thick PTFE mold. Hydrocarbon-based polymers were prepared via melt processing using a commercial laminator (Model LM-404, Astropower Inc.), whereas the silicone specimens were cured in an oven according to the manufacturer's specifications. To promote adhesion to silicone, the quartz was etched in a sulfuric acid:DI (1:1 vol) solution for 12 hours prior to assembly. Furthermore, a commercial primer (92-023, Dow Corning Corp.) was typically used with the silicones to enhance adhesion. The primer was chosen for its good optical bandwidth and lack of haze.

3 Data Reduction

All raw optical measurements were subject to post-analysis. Accounting for all backward and forward reflections, the transmittance through a thick flat-plate at each λ is given by Eq. (5) (Ref. 17)

$$T = \frac{(1 - r_i)^2 e^{-h\alpha}}{1 - \left(r_i^2 e^{-2h\alpha}\right)}, \tag{5}$$

where

$$\alpha = \frac{4\pi k_2}{\lambda}$$

and

$$r_i = \frac{(n_1 - n_2)^2 + \hat{i}\,(k_1 - k_2)^2}{(n_1 + n_2)^2 + \hat{i}\,(k_1 + k_2)^2}.$$

The subscripts 1 and 2 distinguish between materials on opposite sides of the interface. Additional nomenclature includes: T, which represents the optical transmittance {unitless}; r_i, the reflectance at the interface between material 1 and 2 {unitless}; h, the specimen thickness {m}; α, the absorption coefficient $\{m^{-1}\}$; π, the mathematical constant {3.142}; k, the extinction coefficient {unitless}; and n, the real component of the refractive index {unitless}. For air, $n_1 \rightarrow 1.0003$ and $k_1 \rightarrow 0$. Using Eq. (5), all transmitting components were scaled to the common thickness of 3.175 mm for direct comparison, except that $h = 61.25$ mm was used for secondary optics (kaleidoscope homogenizers). The thickness of 3.175 mm corresponds to that of standard "double-strength" ($h = 1/8''$) glass.

Neglecting reflections at the glass/polymer interfaces, the transmittance for a glass/polymer/glass laminate may be analyzed using Eq. (6)

$$T = T_g e^{-h_p \alpha_p}. \tag{6}$$

Here, T_g refers to the transmittance of the glass in air [Eq. (5), for the combined thickness of both silica pieces],

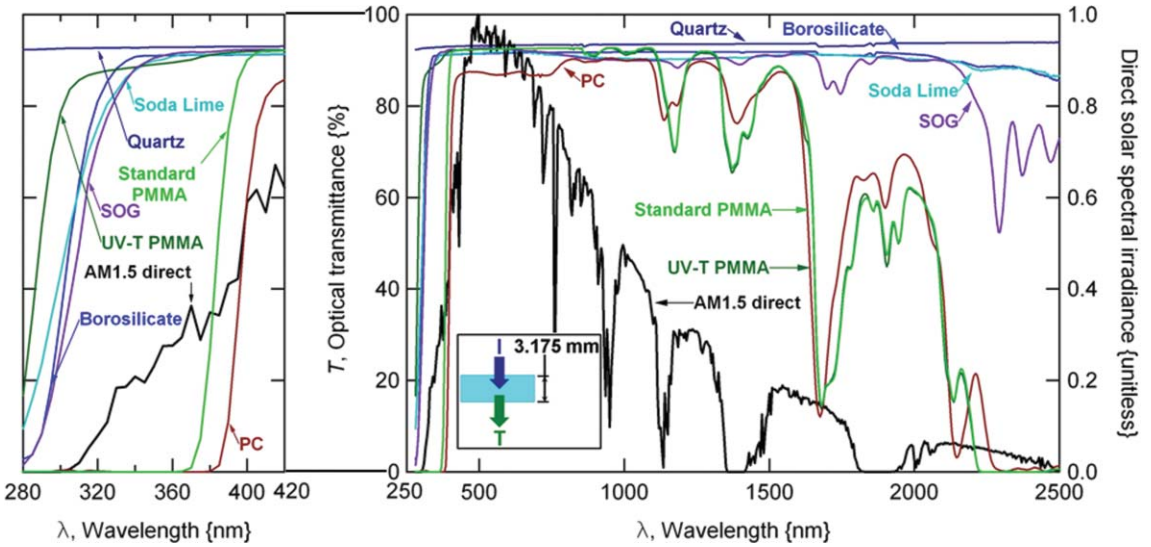

Fig. 2 Measured optical transmittance (in air, scaled to $h = 3.175$ mm) for candidate CPV optical component materials. The results for flat-panel PV (soda-lime glass) as well as the normalized direct solar spectral irradiance (AM1.5 in ASTM G173) are provided for reference.

and the subscript p refers to the polymer. From the numeric solution for α_p at each λ, A, the optical absorptance {unitless} may be determined from Eq. (7)

$$A = 1 - e^{-h_p \alpha_p}. \tag{7}$$

To directly compare the optical measurements from different specimens, A was scaled for $h_p = 0.5$ mm for all polymers including: Poly(methyl methacrylate) (PMMA), Poly(dimethylsiloxane) (PDMS), Poly(phenylmethyl silane) (PPMS), Poly(ethylene-co-methacrylic acid metal salt) (ionomer), EVA, "polyolefin" (PO, a copolymer of polyethylene and polyoctene), Polyvinyl butyral (PVB), and a thermoplastic polyurethane (TPU).

4 Results and Discussion

4.1 *Measurement of Candidate Components and Materials*

4.1.1 *The transmittance of transmitting optics*

The data for several transmitting optical materials is shown in Fig. 2 and further summarized in Table 1. The geometry of the specimens is identified in the inset of the figure. To clarify the nomenclature, the transmitted light is the remainder when the reflected and absorbed portions are subtracted from the incident flux (I), i.e., $T = I - (R + A)$. Figure 2 also includes the normalized direct solar spectral irradiance [AM1.5 in ASTM G173 (Ref. 15)] for reference. The data profiles shown in Fig. 2 are considered representative; each is subject to variation according to the particular material formulation used. A "standard" or specifically UV-transmitting (UV-T) PMMA formulation might be used in a Fresnel lens. Polycarbonate (PC) is sometimes discussed as an alternate material to PMMA for Fresnel lenses. A glass superstrate with silicone facets is another embodiment of the Fresnel lens,[3,18] where the measured spectra for a silicone-on-glass (SOG) lens product is shown in Fig. 2. The glass in the SOG specimen was not tempered, which is shown below (Fig. 3 and Table 4) to improve the performance of a reflector by 1%–2%. A previously solarized low-iron soda-lime glass (noncerium-containing, from Ref. 7) represents the FP-PV superstrate. The term "solarization" refers to the aging of iron, where the spectral transmittance of glass may be affected according to a redox reaction with other trace components, such as cerium or antimony.[3,19,20] Borosilicate or quartz glass may be used to construct lenses or (more typically) secondary optics. Borosilicate glass is known for its low coefficient of thermal expansion (CTE), excellent weatherability, homogeneity, and reasonable cost. In Fig. 2, the standard PMMA, SOG, and borosilicate glass demonstrate a reduced UV transmittance. Quartz is known for its homogeneity and outstanding transmittance across a broad spectrum. Because they are UV-transmitting, components made out of UV-T PMMA or quartz might be used for accelerated UV aging.

All materials in Fig. 2 transmit well over the wavelength range commonly used in MJ CPV cells, i.e., 300–1800 nm. The transmittance for PMMA and PC is significantly reduced in the IR wavelengths not used in the PV application (i.e., >1800 nm, henceforth labeled "UNIR"). A lesser reduction in UNIR transmittance is observed for the SOG specimen, occurring at the same wavelengths as in PMMA. The lesser reduction in UNIR transmittance for SOG is attributed to its structure, i.e., thin silicone facets ($h \sim 0.5$ mm) versus a thick PMMA lens. Reduced transmittance of the NIR spectrum, as in the case of PMMA or SOG, may be beneficial because it will reduce the heating of subsequent components. In Fig. 2, the discrete absorption bands within the AM1.5 terrestrial solar spectrum result from absorption occurring at the source (the sun's Fraunhofer lines[21]) as well as absorption occurring in Earth's atmosphere.[22,23]

Using Eq. (5) at each λ, the transmitted density of unconcentrated direct solar flux (and corresponding maximum current density) is calculated from Eqs. (3) and (4) and reported in Table 1 for the wavelength ranges commonly used in the CPV application as well as the UV and UNIR spectra. Table 1 distinguishes between the separate blue, red, and IR junctions within a III-V cell, where the net φ_T occurs as the sum of each of the three junctions. The reference (direct and global solar) values are calculated for an assumed quan-

Table 1 Summary of measured optical transmittance from Eqs. (3)–(5) of the unconcentrated direct solar spectrum for candidate CPV optical component materials ($h = 3.175$ mm) without AR coatings. In each case, φ or ϕ is weighted relative to the direct solar flux for AM1.5 in ASTM G173, providing a "factor" figure of merit.

	BLUE, 300–650 nm		RED, 650–890 nm		INFRARED, 890–1800 nm		UV, 280–400 nm		UNIR, 1800–2600 nm	
Transmissive	φ_T	φ_T	φ_T	φ_T	φ_T	φ_T	ϕ_T	ϕ_T	ϕ_T	ϕ_T
Material	$\{A \cdot m^{-2}\}$	{%}	$\{A \cdot m^{-2}\}$	{%}	$\{A \cdot m^{-2}\}$	{%}	$\{W \cdot m^{-2}\}$	{%}	$\{W \cdot m^{-2}\}$	{%}
PC	170	81	200	89	320	80	5.9	18	7.6	23
Standard PMMA	190	87	210	93	330	81	8.5	27	7.1	22
Borosilicate glass	190	90	210	92	370	92	29	90	29	89
Soda-lime glass	190	90	210	92	370	91	29	89	29	89
UV-T PMMA	190	91	210	93	330	81	29	90	7.0	22
SOG	190	91	210	92	360	90	29	89	26	81
Quartz glass	200	92	210	94	380	94	30	93	30	93
Direct solar	213.0	100	223.5	100	402.7	100	32.0	100	32.3	100
Global solar	249.7	117	243.8	109	421.3	105	51.9	149	32.6	101

tum efficiency of 100% throughout the wavelengths specified in Table 1. To aid comparison within a wavelength region, the theoretical maximum current density and optical energy fluxes are specified in Table 1 as a percentage of the direct solar flux in addition to their nominal values. Materials are ranked in the table according to the φ_T of the blue junction, with the most-transmitting being at the bottom of Table 1. Throughout the study here, the current-limiting condition was found to be anticipated for the blue junction. As in Fig. 2, T is calculated in Table 1 for $h = 3.175$ mm for specimens without any antireflective (AR) coating(s) present.

Of the materials considered, quartz has the best transmittance in each band of wavelengths. Reduced transmittance in the application-specific wavelengths for c-Si and MJ cell technology primarily occurs in the shorter wavelengths for standard PMMA, PC, soda-lime glass, and SOG. For these materials, some loss occurs in addition to the ~4% reflectance at each of the free surfaces. Specifically, the optical cut-on within the UV wavelengths reduces the transmittance within the range of the blue junction more than that within the range of the red junction. The properties of the optics alone do not solely determine the current-limiting junction. For example, during a cloudless day, more red colorcast is present at

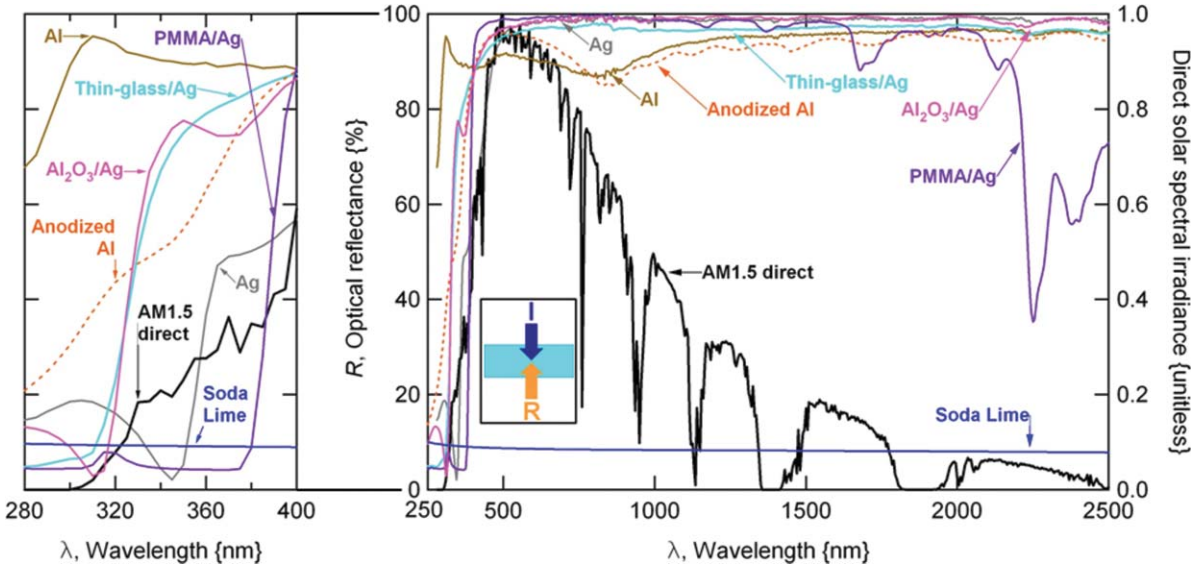

Fig. 3 Measured optical reflectance (absolute, for direct normal incidence in air) for candidate CPV optical component materials. The normalized direct solar spectral irradiance (AM1.5 in ASTM G173) is provided for reference.

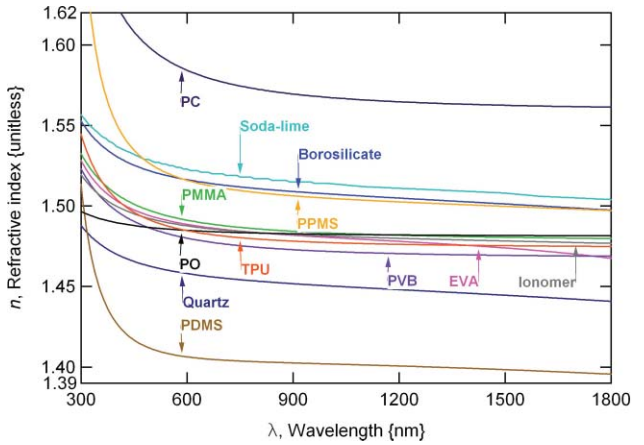

Fig. 4 Real refractive index (n, measured or from a trendline fit) for candidate CPV optical materials over the wavelength range commonly used in CPV. The result for FP-PV (solarized soda-lime glass) is provided for reference.

sunrise and sunset, whereas a blue colorcast is present during the middle of the day. Of the materials in Fig. 2, only standard PMMA demonstrates significantly reduced transmittance of the terrestrial UV spectrum based on its cut-on λ of $\sim$390 nm. Of the materials in Fig. 2, the PMMA and PC formulations demonstrate the lowest transmittance in the AM1.5 ASTM G173 NIR spectrum. Note that a small portion (cumulative flux of 7.8 $\mathrm{W \cdot m^{-2}}$) of the AM1.5 ASTM G173 direct spectrum exists for $\lambda = 2600$–4000 nm. Because the bottommost (Ge) junction in MJ technology is seldom current-limiting, the transmittance above 1000 nm (where some absorptance occurs for most of the materials) is generally not consequential to power harvesting. That is, from Table 1, the infrared junction would not be expected to become current-limiting for PMMA or PC. In addition to the lesser spectral bandwidth and lesser optical transmittance in Fig. 2 and Table 1, PC has known vulnerability to terrestrial solar UV induced photooxidation (facilitated by a photo-Fries rearrangement).[24–26] All of these issues have historically precluded the use of PC in CPV lenses.

Relative to Ref. 12, where the "direct solar" (theoretical maximum) values are $\varphi_T = 596.5$ $\mathrm{W \cdot m^{-2}}$ and UNIR $\phi_T = 175.5$ $\mathrm{W \cdot m^2}$ for c-Si, the values in Table 1 for the blue, red, and IR junctions sum to $\varphi_T = 840.8$ $\mathrm{W \cdot m^{-2}}$ and UNIR $\phi_T = 32.1$ $\mathrm{W \cdot m^2}$. That is, a greater portion of IR light is used in MJ technology, where the wavelength region that may be harvested extends up to 1800 nm (instead of 1120 nm for c-Si). The aforementioned difference implies that as much as 41% more energy may be generated from the terrestrial spectrum using a MJ cell. The greater optical bandwidth for MJ cells (those typically used in CPV systems with high C_g) implies that 82% less of the incident optical flux is available to heat the cell (or reflect back to the encapsulant).

For MJ cells, PMMA is in all cases the least IR-transmitting, including absorption in the IR that cannot be harvested by c-Si cells. The majority of the presently available commercial MJ cells, however, are not specifically designed for compatibility with PMMA optics[27] (where UV and blue light are attenuated), therefore power production is more likely limited at the blue junction. Further comparing Table 1 to Ref. 12, the materials are similarly ranked between c-Si and MJ technologies in the UV and UNIR wavelengths. The same UV wavelengths are examined in Table 1 and Ref. 12.

4.1.2 *The effect of AR coatings on optical transmittance*

The two common approaches (graded index or optical interference)[28,29] are represented in Table 2, quantifying the effect of AR coatings on transmittance. Table 2 identifies the improvement in transmittance (maximum current density for normal incidence, relative to an uncoated glass specimen) of the ASTM G173 direct solar spectrum within the blue, red, infrared (or total for c-Si), UV, and UNIR wavelengths. A graded-index coating may use either a density that varies with depth or a microscale surface texture resembling the structure found in a moth eye.[30] The graded-index coating in Table 2 consists of a single material (silica), where the porosity is increased toward the free surface. Optical interference refers to the cancelation of reflected flux (occurring at $h = \lambda/4$ for a single thin film), where the bandwidth of the coating may be extended using multiple thin films. Two multilayer laminate interference coating designs are examined in Table 2, each tailored specifically to c-Si or MJ cell technology. Although the values in Table 2 are representative, the performance of an interference filter is very much subject to its design and implementation, i.e., the number and thickness of the layers.

Foremost, the effect of an AR coating is to improve transmittance by 2%–3% per coated surface, which may be used to increase power production at the cell. The graded-index coating is expected to better enhance power production when used with a c-Si cell, because the coating has a greater optical bandwidth approaching the range of wavelengths that may be harvested by c-Si. Furthermore, improved transmittance may occur at a broader range of incident angles, more

Table 2 Comparison of the change in transmittance (relative to uncoated glass) associated with typical AR technology products.

AR Technology	c-Si CELL, 300–1120 nm φ_T {%}	c-Si UNIR, 1120–2600 nm, ϕ_T {%}	BLUE, 300–650 nm φ_T {%}	RED, 650–890 nm φ_T {%}	INFRARED, 890–1800 nm φ_T {%}	UV, 280–400 nm ϕ_T {%}	III-V UNIR, 1800–2600 nm ϕ_T {%}
Graded Index	2.7	1.8	1.7	3.3	2.5	1.3	0.7
Interference	2.0	– 7.6	N/A	N/A	N/A	– 22.9	N/A
Interference	N/A	N/A	2.1	2.7	– 6.7	– 17.2	– 9.1

consistent with the global solar spectrum relevant to FP-PV. Between the particular coatings examined in Table 2, the interference coating is expected to better enhance power production when used with the MJ cell technology. To explain, the blue junction benefits more from the interference than the graded-index coating. The blue junction is critical as it was seen to be the most limiting of the materials examined in Table 1. The graded-index filter will also enhance the transmission of UV and IR flux not used in power production. The interference filter, however, attenuates the unused UV and IR flux and therefore might improve the reliability of an encapsulation material because it acts as a dichroic filter, limiting the UV and UNIR dose.

4.1.3 *The refractive index of transmitting optics*

The refractive index for optical component or encapsulant materials is shown in Fig. 4. The data were obtained from material manufacturers, commercial software,[31] or a separate laboratory[32] and were not independently verified at NREL. n is either directly measured using ellipsometry or extracted from a published trend-line fit (such as Cauchy's dispersion law or the Sellmeier equation[17]). For Fig. 4, n was sometimes extrapolated from 1550 to 1800 nm to match the range of the CPV application. From Eq. (5), reflective losses are minimized when n is similar between adjacent materials. Therefore, the greatest reflectance loss occurs at any air/material interface. For the typical materials shown in Fig. 4, however, the maximum reflectance of ~0.2% per interface is expected for an n mismatch of 0.13, e.g., a glass/PDMS interface. PPMS is instead particularly well-matched to borosilicate and soda-lime glass. The use of PPMS as an encapsulant, however, is not recommended because the aromatic phenyl ring structure is known to yellow in response to UV photoexcitation.[33–35] Separately, PMMA, EVA,PVB, TPU and ionomer all demonstrate very similar n. While generally similar in magnitude to the other hydrocarbon materials, PO does not vary as substantially with wavelength. The use of a fluid to fill the module cavity, thereby reducing the reflectance losses of the internal components, is not considered in this study.

The Sellmeier fitting coefficients, Eq. (8), and dispersion [Abbe number, Eq. (9)] of the candidate CPV optical materials are provided in Table 3

$$n^2 - 1 = \frac{B_1\lambda^2}{\lambda^2 - C_1} + \frac{B_2\lambda^2}{\lambda^2 - C_2} + \frac{B_3\lambda^2}{\lambda^2 - C_3}. \tag{8}$$

$$V = \frac{(n_D - 1)}{(n_F - n_C)}. \tag{9}$$

New parameters in the equations include the fitting coefficients, B $\{\mu m^{-2}\}$ and C $\{\mu m^2\}$, and the Abbe number, V {unitless}. The Sellmeier coefficients were obtained using a least-squares fit of the data in Fig. 4 and are included here to aid optical modeling. V was determined using the Sellmeier coefficients at the wavelengths of 589.3 nm (D), 486.1 nm (F), and 656.3 nm (C). Those materials with a small V, such as PPMS in Table 3, typically demonstrate the greatest change in n with λ, whereas those materials with the largest V, i.e., ionomer and PO, exhibit the least dispersion. Note that n (therefore, T and A) will vary according to behavior of additives, which may include fillers such as glass.

Aside from index matching, the materials in Fig. 4 all demonstrate normal dispersion [a steep rise (or inflection) in n at the left of the Fig. 4]. A difference in the location of λ_i, the wavelength of the inflection, would result in increased reflectance loss from optical mismatch between adjacent materials for $\lambda \leq \lambda_i$. More importantly, normal dispersion will retard light as λ is decreased. For Fresnel optics, this results in chromatic aberration, where shorter wavelengths will be focused closer to the lens; conversely, longer wavelengths will be focused farther from the lens. For Fresnel-based systems, common methods used to minimize chromatic aberration include: curving the lens to reduce the optical path

Table 3 Sellmeier coefficients and Abbe number for candidate CPV optical materials.

Material	B_1 $\{\mu m^{-2}\}$	B_2 $\{\mu m^{-2}\}$	B_3 $\{\mu m^{-2}\}$	C_1 $\{\mu m^2\}$	C_2 $\{\mu m^2\}$	C_3 $\{\mu m^2\}$	V, Abbe # {unitless}
PC	1.002E + 00	4.274E − 01	− 1.371E + 31	6.990E − 03	4.449E − 02	7.544E + 36	29
PPMS	3.013E − 01	9.576E − 01	7.965E + 01	6.330E − 02	− 8.682E − 03	1.240E + 04	35
TPU	8.554E − 01	3.170E − 01	6.817E + 01	2.338E − 02	− 3.419E − 02	− 2.840E + 07	51
PVB	7.787E − 01	3.741E − 01	− 5.602E − 02	1.274E − 02	8.392E − 03	3.875E + 02	53
PDMS	3.961E − 01	5.793E − 01	− 7.422E + 00	5.001E − 02	− 4.049E − 02	− 8.939E + 02	55
Standard PMMA	7.573E − 01	4.309E − 01	2.099E + 00	1.395E − 02	4.266E − 03	3.106E + 03	57
EVA	7.594E − 01	4.301E − 01	4.374E − 02	1.770E − 02	− 8.959E − 03	6.879E + 00	62
Borosilicate Glass	8.020E − 01	4.695E − 01	1.110E + 00	4.130E − 03	1.605E − 02	1.133E + 02	64
Soda-lime Glass	8.098E − 01	4.810E − 01	2.957E + 00	8.886E − 03	8.085E − 03	2.945E + 02	65
Quartz	6.708E − 01	4.333E − 01	5.840E − 01	4.515E − 03	1.327E − 02	6.439E + 01	68
Ionomer	7.935E − 01	3.950E − 01	4.715E + 00	1.366E − 02	− 5.156E − 03	1.498E + 03	74
PO	7.957E − 01	3.979E − 01	− 4.522E − 01	4.075E − 03	1.896E − 03	1.197E + 04	184

length between the lens and cell;[36] use of a high n fluid to fill the module cavity—if V is reasonably matched to the system to reducing dispersion-related index mismatch; using a nonimaging lens design where the lens facets mix the colors; and the addition of a secondary optic to render a more homogeneous spectral distribution.[36] The V in Table 3 exceeds that of many of the polymers, e.g., $V = 30$ for PC,[31,37,38] where the greater dispersion would enhance chromatic dispersion. For encapsulants, the dispersion may aid the reflection of damaging UV light at an interface along the optical path, possibly at the expense of localized current mismatch in MJ cells.

4.1.4 *The reflectance of reflecting optics*

The measured data for several optical reflector components is shown in Fig. 3 and further summarized in Table 4. Reflectors considered include: a sputtered Ag film (Ag); sputtered Al (Al) film; a wet-silvered (on the second surface) low-iron glass ($h = 4$ mm) composite (thick-glass/Ag); wet-silvered (second surface) tempered low-iron glass ($h = 4$ mm, tempered thick-glass/Ag); wet-silvered (second surface) low-iron glass ($h = 1$ mm, thin-glass/Ag); a PMMA superstrate/Ag composite (PMMA/Ag); PMMA superstrate/adhesive/Ag (PMMA/adhesive/Ag); an anodized aluminum composite (anodized Al); a 1.5-μm Al_2O_3 thin-film/Ag first surface composite (Al_2O_3/Ag) deposited on Polyethylene terephthalate (PET); a 1.5-μm SiO_2 thin-film/Ag first surface composite (SiO_2/Ag) deposited on PET; and soda-lime glass. To clarify, the nomenclature used in Fig. 3 and Table 4 refers only to the essential component layers, indicated from the first (incident) side to the second (back) surface. The primary reflective interface for the specimens in Fig. 3 and Table 4 occurs at an Ag or Al layer, facilitated by their known high reflectance across a broad spectrum. Other materials such as Pt, Fe, Ni, Cr, Rh, and $BaSO_4$ provide a lower base reflectance or fail to reflect at shorter wavelengths, like Au. The profile for soda-lime glass comes from the analysis [$2r_i$ in Eq. (5)] of published n and k data,[39]As with the transmittance data, Fig. 2, the reflectance data applies to optical components in their unconditioned initial state; degradation over time (owing to mechanisms including corrosion, abrasion, soiling, and photodegradation) is examined elsewhere.[3,13,40] As with the transmittance data, the subsequent scattering of light caused by the optical component (known as haze) is not considered here, nor is the state of optical polarization.

Consistent with Ref. 17, bare Ag has a cut-on λ near 360 nm, whereas bare Al is more reflecting to UV but demonstrates reduced reflectance centered at about $\lambda = 775$ nm. The PMMA/Ag profile demonstrates the typical absorptance seen in polymeric materials such as the PMMA or SOG components in Fig. 2. As indicated in the soda-lime profile in Fig. 3, the typical reflectance of transmitting components, i.e., glass or PMMA in Table 1, is ~4%/surface. From Table 2, an AR coating may decrease the reflectance of glass sheet to ~1%/surface (total R of 2%).

Like Table 1, the reflected flux density (and corresponding maximum current density) from Eqs. (3) and (4) for a single pass of unconcentrated direct solar radiation is provided in Table 4. Table 4 is ranked according to reflectance in the blue wavelengths expected to limit the current in a MJ cell. Over $\lambda = 300$–1800 nm, an average hemispherical reflectance of 94.3 and 92.6% is observed for bare Ag and Al, respectively. Because of loss at lower or intermediate wavelengths, these values slightly exceed the average reflectance over $\lambda = 300$–1120 nm, i.e., 90.6 and 90.1%, respectively. In Table 4, Ag is a superior reflector over Al in the profiles as in Fig. 3 except in the UV wavelengths. The greater UV reflectance for Al-enabled mirrors in Fig. 3 suggests they could be used in accelerated aging equipment, particularly to enhance the UV dose relative to PMMA refractive- or Ag reflective-optical systems. All of the components in Table 4 demonstrate strong reflectance in the application-specific wavelengths as well as the UNIR spectrum. The PMMA/Ag and PMMA/adhesive/Ag specimens are the least UNIR-reflecting. Tempering glass, commonly used in FP-PV to improve impact durability, slightly improves reflectance in the blue, red, and UV wavelengths (Table 4 and Ref. 13). The improvement in transmittance is speculated to come from the relaxation of stress and/or alteration of the glass modifiers (changes in chemistry or location relative to the material network) occurring during the high-temperature anneal. A PMMA superstrate (containing UV stabilizers) reduces the reflected blue and UV wavelengths. Performance of PMMA/Ag is subject to the additional layers (such as the adhesive) used in the mirror stack (Table 4). Al_2O_3/Ag provided the best performance specific to the PV application. Al_2O_3/Ag might substitute particularly well in CPV systems using an internally located reflective secondary homogenizer, where the component would be mechanically and chemically protected from the environment.

Comparing Table 4 to Ref. 12, the propagated spectrum of the candidate materials is similar between c-Si and MJ cell technology. The rank is notably lesser in Table 4 (indicating reduced φ_R) for SiO_2/Ag and PMMA/adhesive/Ag (where the adhesive reduces reflectance relative to PMMA/Ag). The rank is notably greater in Table 4 (indicating increased φ_R) for tempered thick-glass/Ag and thin-glass/Ag. Furthermore, the Ag-enabled reflectors consistently scored higher than those using Al, despite the lesser reflectance of the Ag base layer in the UV wavelengths. Regarding the rank according to the reflectance in the blue wavelengths, the Al and anodized Al specimens are exceptions—the reduced reflectance about $\lambda = 775$ nm would favor a current-limiting condition at the red junction. Between Table 4 and Ref. 12, the rank (sorted by ϕ_R in the UNIR wavelengths) is improved in Table 4 for anodized Al (relative to tempered thick-glass/Ag) and sputtered Al (relative to 1.5 μm Al_2O_3/Ag). The aforementioned changes in the UNIR ranking of the materials are not significant, being on the order of a few percent.

4.1.5 *The optical absorptance of encapsulation materials*

Applying Eq. (6) and then Eq. (7), the absorptance of several encapsulation materials is shown in Fig. 5 and further summarized in Table 5. The geometry of the specimens is identified in the inset of Fig. 5. While a thickness similar to $h = 3$ mm is commonly used in refractive components (Fig. 2), PMMA is analyzed in Fig. 5 for $h = 0.5$ mm, so that it may be directly compared to the encapsulants. The most-transmitting of multiple formulations (as many as 14 separate specimens of a particular polymer were examined) was chosen for Fig. 5 and Table 5. The data presented is, however, considered representative; polymeric materials are subject

Table 4 Summary of measured optical reflectance (corrected to absolute) from Eqs. (3) and (4) of the unconcentrated direct solar spectrum for candidate CPV optical materials. In each case, the theoretical maximum current density (φ) or optical flux density (ϕ) values are listed in addition to their proportion of the direct solar flux for AM1.5 in ASTM G173, providing a "factor" figure of merit.

	Blue, 300–650 nm		Red, 650–890 nm		Infrared, 890–1800 nm		UV, 280–400 nm		UNIR, 1800–2500 nm	
Reflective Material	φ_R {A·m^{-2}}	φ_R {%}	φ_R {A·m^{-2}}	φ_R {%}	φ_R {A·m^{-2}}	φ_R {%}	ϕ_R {W·m^{-2}}	ϕ_R {%}	ϕ_R {W·m^{-2}}	ϕ_R {%}
Soda-lime glass	18	8.6	19	8.5	33	8.2	2.9	9.1	2.6	8.0
1.5 μm SiO_2/Ag	180	83	220	97	390	98	17	52	32	98
PMMA/adhesive/Ag	190	89	220	99	390	96	5.1	16	26	80
Al (sputtered)	190	89	200	89	380	94	28	89	31	96
Anodized Al	200	92	200	89	370	92	22	69	31	95
Thick-glass/Ag	200	92	210	96	380	94	25	78	29	91
Ag (sputtered)	200	92	220	100	400	98	18	55	32	99
PMMA/Ag	200	93	220	100	390	97	7.4	23	25	77
Thin-glass/Ag	200	93	220	98	390	96	24	76	31	97
Tempered thick-glass/Ag	200	94	220	96	380	94	26	80	29	90
1.5 μm Al_2O_3/Ag	200	94	220	100	400	99	23.5	73	32	98
Direct solar	213.0	100	223.5	100	402.7	100	32.0	100	32.3	100
Global solar	249.7	117	243.8	109	421.3	105	51.9	149	32.6	101

to the formulation used, including: initiators, photostabilizers, UV absorbers, antioxidants, adhesion promoters, curing agents, and overall compositional purity. A key assumption regarding Eq. (6) is that no significant internal reflections occur within the laminate specimens at the glass/polymer interface. To explain, n is assumed to be similar for the glasses and polymers (as in Fig. 4), while k is assumed to be negligible (as is typical in highly transmitting materials).

Many of the materials in Fig. 5 demonstrate some absorptance of UV light, likely caused by additives including the UV stabilization system. UV absorptance should therefore not be confused with propensity for photodegradation or overall resistance to UV damage. The materials in Fig. 5 also demonstrate NIR absorptance, enabling the material to be directly heated by the sun. Absorption peaks at 900–940 nm, 1000–1050 nm, 1100–1300, and

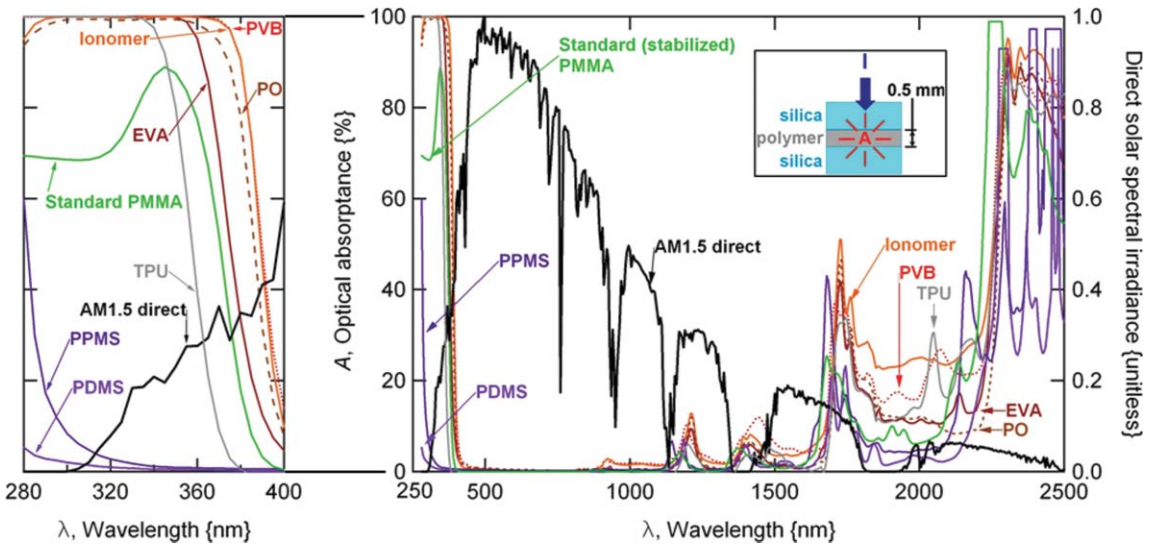

Fig. 5 Optical absorptance [from Eq. (6) then Eq. (7), in air, scaled to $h = 0.5$ mm] for candidate CPV encapsulant materials. The normalized direct solar spectral irradiance (AM1.5 in ASTM G173) is provided for reference.

Table 5 Optical absorptance calculated using Eqs. (3), (4), (6), (7), and the direct AM1.5 solar spectrum (ASTM G173) for candidate CPV encapsulation materials for $h = 0.5$ mm.

	BLUE, 300–650 nm		RED, 650–890 nm		INFRARED, 890–1800 nm		UV, 280–400 nm		UNIR, 1800–2600 nm	
Encapsulation Material	φ_A $\{A \cdot m^{-2}\}$	φ_A {%}	φ_A $\{A \cdot m^{-2}\}$	φ_A {%}	φ_A $\{A \cdot m^{-2}\}$	φ_A {%}	ϕ_A $\{W \cdot m^{-2}\}$	ϕ_A {%}	ϕ_A $\{W \cdot m^{-2}\}$	ϕ_A {%}
PPMS	0.0	0.0	0.0	0.0	11	2.6	0.1	0.3	7.4	23
UV-T PMMA	0.1	0.0	0.1	0.0	12	3.0	0.1	0.3	14	45
PDMS	0.1	0.1	0.0	0.0	8.5	2.1	0.1	0.4	6.7	21
Standard PMMA	6.2	2.9	0.1	0.0	12	3.0	15	45	13	41
EVA	7.8	3.7	0.0	0.0	14	3.6	19	59	11	35
Poly-α-olefin (PO)	8.3	3.9	0.0	0.0	11	2.7	23	73	10	30
Ionomer	9.2	4.3	0.0	0.0	15	3.6	25	79	14	44
PVB	11	5.1	0.0	0.0	16	4.0	26	80	13	41
TPU	12	5.8	0.2	0.1	18	4.5	27	84	13	41
Direct solar	213.0	100	223.5	100	402.7	100	32.0	100	32.3	100
Global solar	249.7	117	243.8	109	421.3	105	51.9	149	32.6	101

1650–1750 nm are attributable to C-H absorptions due to vibrational overtones and combination bands of NIR peaks occurring at lower wavenumbers.[40,41] Additional absorptance at 1.4, 1.9, and 2.7 μm may occur when water is present in the polymer.[40,42,43] Regarding NIR absorptance, potential hazards include direct thermal or hydrothermal degradation at sufficient temperatures. Perhaps more commonly, temperature is coupled to UV photodegradation. The activation spectrum can therefore be readily influenced by the specimen temperature, e.g., the prevalent damage modes can significantly vary with temperature.[44] Likewise, the rank of the most robust materials can vary with temperature.[44] For the encapsulation materials of the geometry shown in the inset of Fig. 5, the absorbed flux density (and corresponding maximum current density) of unconcentrated direct solar radiation is provided in Table 5. PDMS, which has the greatest n mismatch in Fig. 4, is the least absorbing in almost every band of wavelengths except the blue (used to rank Table 5). PDMS, PPMS, and PMMA are the materials least absorbing in the blue, red, and IR wavelengths, enabling the greatest power production. In contrast, ionomer, PVB, and TPU demonstrate the greatest absorptance in the PV as well as the UV and UNIR wavelength bands. The efficacy of UV photodegradation of polymeric materials is evaluated below. In contrast, the temperature of components adjacent to the cell is very much dependent upon the module's thermal management design. Consider also that much of the optical flux not absorbed in Table 5 will be accommodated at the cell (either directly or through thermalized photon absorptance of light above the semiconductor bandgap energy) in addition to Joule heating of the interconnects. Note that other factors such as the specific formulation or grade of material may affect the results in Table 5.

Minor differences exist between the candidate materials when used with c-Si or MJ cell technology. In particular, the rank of PPMS and PDMS is opposite in Table 5 relative to Ref. 12 for φ_A. All of the materials in Table 5 are more absorbing in the blue than the red wavelengths (where absorptance is minimal), favoring the current-limiting condition for the blue junction. Absorptance increases in the IR and UNIR wavelengths, favoring direct heating of the encapsulation. When sorted by ϕ_R in the UNIR range, TPU is more absorbing for $\lambda = 1800$–2600 nm than ionomer and PVB, respectively.

Of the encapsulants considered here, EVA has traditionally dominated the FP-PV application on the basis of its low cost and good optical performance. All of the materials in Table 5, however, were considered as candidate encapsulants based on their excellent optical clarity, where minor differences are accentuated when φ_A is examined as a percentage of the direct solar resource. During their service life, EVA formulations are subject to aging, affecting optical characteristics[45–47] as well as adhesion[7] over time, further resulting in the formation of acetic acid.[48] EVA has found application in FP-PV not because it provides the best optical performance or overall durability; rather, it provides a practical compromise between performance, durability, and cost. In contrast, it is presently unclear which material(s) are best suited for the CPV application. However, in a concentrating system, a lesser volume of encapsulation material is used, therefore the significance of cost is reduced relative to performance and reliability, favoring PDMS.

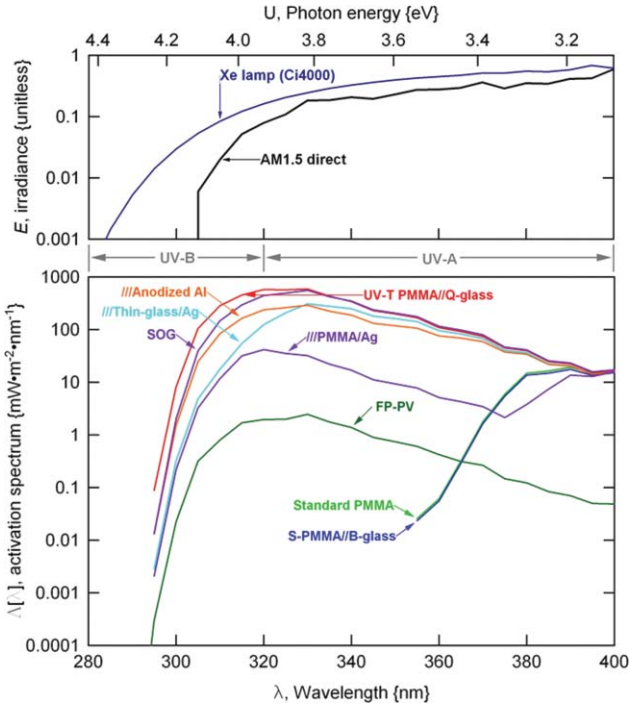

Fig. 6 From Eqs. (1), (2), and (10), Λ (at $C_g = 500$, except for FP-PV) for key representative optical systems. The normalized spectral irradiance profiles for the direct solar resource (AM1.5 in ASTM G173) as well as a Xe lamp are provided for reference. The "UV-A" and "UV-B" bands are indicated at the top.

4.2 *Damaging Radiation for a Polymeric Encapsulant: The Effective UV Damage Dose and NIR Flux*

4.2.1 *The damaging UV radiation at the encapsulation*

The effective dose of damaging radiation, Eq. (2), may be determined from the activation spectrum, Eq. (1). As indicated in Fig. 1, the spectral irradiance at the front surface of the polymeric encapsulation may be estimated from the series of preceding transmittance and/or reflectance events occurring within the optical system, Eq. (10).

$$E[\lambda] = E_I[\lambda] C_g \prod_{i=1}^{i=j} \eta_i T_i[\lambda] \prod_{k=1}^{k=l} \eta_k R_k[\lambda]. \quad (10)$$

Here, η represents the optical efficiency {unitless}; R, the reflectance at a mirror component {unitless} in addition to the indices i, j, k, and l. The term E_I refers to the incoming radiation (global solar, Xe lamp, or direct normal solar) incident upon the optical system. The optical efficiency, η, was assumed to be 0.95 for both refractive and reflective optical systems. In a Fresnel lens, optical loss may occur due to the finite draft angle, tip radius, and valley radius of the lens facets. In a reflector, loss may occur due to the mechanical attachment, view factor, and nonspecularity of reflection. Transmittance for secondary homogenizer optic components ($\eta = 0.99$, assumed for total internal reflection) was calculated using Eq. (5) for $h = 61.25$ mm using the T data measured at each λ (for a 5-nm increment) for stock glass.

The modeled activation spectra, $\Lambda[\lambda]$, for several concentrating optical systems is shown in Fig. 6; the UV energy flux, UNIR energy flux, and effective UV dose [Eqs. (1)–(4)] are further summarized in Table 6. Figure 6 includes profiles for soda-lime glass with no concentration (FP-PV), a standard PMMA lens (Standard PMMA), a CPV SOG lens (SOG), a standard PMMA lens/borosilicate glass homogenizer system (S-PMMA/B-glass), a UV-T PMMA lens/quartz homogenizer system (UV-T PMMA/Q-glass), a soda-lime front glass/wet-silvered low-iron 1-mm-thick glass reflector (///thin-glass/Ag), a front glass/PMMA superstrate/Ag reflector (///PMMA/Ag), and a front glass/anodized aluminum reflector (///anodized Al). The nomenclature / is used to distinguish between the primary components within a composite construction, // identifies an air-gap between components, and /// identifies a soda-lime front glass followed by an air gap.

The UV-T PMMA//Q-glass system, which may be used to greatly accelerate photodegradation for investigating candidate materials, provides the greatest dose of damaging radiation. A similar exposure would be realized if UV-T PMMA were replaced by an SOG lens (Fig. 6 and Table 6). The ///anodized Al, ///thin-glass/Ag and flat panel (simply a soda-lime glass superstrate) systems have $\Lambda[\lambda]$ profiles similar in shape but differing in magnitude (note logarithmic scale). The standard PMMA lens (used on its own or with a borosilicate glass homogenizer) has a $\Lambda[\lambda]$ profile that rapidly decreases toward the left of Fig. 6, where it becomes limited by the cut-on wavelength at 390 nm.[40] Although the profile for S-PMMA/B-glass is clearly attenuated relative to Standard PMMA in Fig. 6 for $\lambda \leq 335$ nm, the homogenizer does not greatly affect the overall damage dose in Table 6. The reflector components (thin-glass/Ag, PMMA/Ag, and anodized Al) all provide UV damage dose greater than a Standard PMMA lens, Fig. 6. The PMMA/Ag reflector is the least damaging of the reflectors shown in Fig. 6. The Standard PMMA refractor or reflector components represent commonly employed "low-concentration" CPV systems, i.e., $C_g \leq 50$. The PMMA lens//borosilicate homogenizer system or reflector//borosilicate homogenizer systems represent commonly employed CPV configurations for "medium" to "high" concentration, i.e., $C_g \geq 50$.

The expected maximum current density, UV damage dose, and UNIR energy flux for representative optical systems are summarized in Table 6. For the representative optical systems, Eqs. (3), (4), and (10) are used together to calculate the transmitted maximum current density, φ_T, where the PV Effective C_g identifies the maximum current density relative to the nominal C_g. The Rank is listed to identify the greatest φ_T or ϕ_T (in order from least the greatest). Rank is listed separately for the blue, red, and IR junctions as well as the UNIR ϕ_T because the systems in Table 6 are listed in order of their effective dose of UV radiation, D. Equations (1) and (2) were also used to calculate the UV Dose Factor, which identifies D relative to C_g. In Table 6, the UV dose for FP-PV, calculated for the ASTM G173 global solar irradiance, is used as a reference and compared to two Xe-lamp-accelerated test conditions commonly used at NREL. Specifically, the Xe lamp is maintained at 2× the ASTM G173 global E_I at $\lambda = 340$ nm or at 2.5× the global E_I ($\phi = 114$ W·m^{-2}) for $\lambda = 300$–400 nm. In addition to the added irradiance, an additional 3–4× acceleration can be achieved for indoor aging, since the lamp may be continuously operated for 24 hours/day.

Table 6 Summary of theoretical maximum current density, UV activation spectrum analysis [from Eqs. (1)–(4) and (10)], and UNIR energy flux for representative optical systems subject to the direct solar spectrum; the dose "factor" compares the system dose to that of FP-PV subjected to the global solar spectral irradiance (AM1.5 in ASTM G173) or a FP-PV subjected to a Xe lamp.

		Blue, 300–650 nm			Red, 650–890 nm		Infrared, 890–1800 nm		280–400 nm	UNIR, 1800–2500 nm		
	C_g, Geometric	φ_T,	Effective	Rank	φ_T,	Effective	φ_T,	Effective	UV Dose	ϕ_T,	Effective	Rank
	Concentration	$\{A \cdot m^{-2}\}$	C_g	{unitless}	$\{A \cdot m^{-2}\}$	C_g	$\{A \cdot m^{-2}\}$	C_g	Factor	$\{kW \cdot m^{-2}\}$	C_g	{unitless}
System	{unitless}		{unitless}			{unitless}		{unitless}	{unitless}		{unitless}	
Global solar/soda-lime **(FP-PV, field application)**	1	0.24	1.1	1	0.24	1.1	0.40	1.0	1.0	0.03	1.0	3
Xe-lamp/soda-lime **(FP-PV, accelerated indoor aging)**	2 @ 340 nm	0.40	1.9	2	0.76	3.4	0.92	2.3	2.7	0.00	0.0	1
Xe-lamp/soda-lime **(FP-PV, accelerated indoor aging)**	2.5 @ 300–400 nm	0.44	2.1	3	0.84	3.8	1.02	2.5	3.0	0.00	0.0	2
Standard PMMA/anodized Al homogenizer	500	80	400	9	90	400	140	350	4.3	3.2	110	7
Standard PMMA lens/borosilicate homogenizer	500	80	380	5	90	410	140	340	4.7	11	360	13
Standard PMMA lens	500	90	420	11	100	450	150	380	5.2	2.9	100	5
///PMMA/Ag reflector/borosilicate homogenizer	500	80	390	7	90	420	160	400	8.8	12	410	14
///PMMA/Ag reflector	500	90	420	15	100	460	180	440	20	13	420	15
///thin-glass/Ag//thin-glass/Ag//borosilicate homogenizer	500	70	350	4	90	380	150	360	60	3.3	110	8
///Anodized Al/borosilicate homogenizer	500	80	390	6	80	380	150	370	80	14	450	18
///Ag reflector (sputtered)	500	90	420	13	100	460	180	440	90	7.7	250	11
///thin-glass/Ag/borosilicate homogenizer	500	80	390	8	90	410	160	390	90	14	450	17
///thin-glass/Ag	500	90	430	16	100	450	180	430	130	14	450	19
///thick-glass (tempered)/Ag	500	90	430	17	100	440	170	420	130	7.8	260	12
///Anodized Al	500	90	420	12	90	410	170	410	140	13	450	16
///Al reflector (sputtered)	500	90	410	10	90	410	170	420	240	14	460	20
SOG lens	500	90	440	20	100	450	170	430	250	6.6	220	9
Borosilicate lens	500	90	430	18	100	450	180	440	270	3.0	100	6
UV-T PMMA lens/quartz homogenizer	500	90	420	14	100	440	150	370	270	7.2	240	10
UV-T PMMA lens	500	90	440	19	100	450	150	380	280	2.2	70	4
Direct solar (bare cell)	1	0.213	1.00	N/A	0.224	1.00	0.403	1.00	0.68	0.032	1.07	N/A
Global solar (bare cell)	1	0.250	1.17	N/A	0.244	1.09	0.421	1.05	1.19	0.033	1.08	N/A

Regarding the transmitted UV flux in particular systems, the instantaneous UV dose from the Xe lamp(s) is of the same order of magnitude as that encountered when a standard PMMA Fresnel lens is used at $C_g = 500$. The Fresnel lens in Fig. 6 and Table 6 provides a greater dose (5.2 versus 4.6) than the idealized stock specimen in Ref. 12; such variation might be expected based on the variety of thickness and PMMA formulations used in CPV lens products. A significantly greater UV dose is anticipated for UV transmitting optics (UV-T-, borosilicate, quartz, or SOG lenses). Here, the UV dose factor is still considerably less than that anticipated from the nominal C_g, in part because a significant portion of diffuse UV light present in the global solar spectrum is not present in the direct solar spectrum (concentrating optics can only focus direct light). For SOG, where PDMS is known to be UV-transmitting (Fig. 5), ~50% of the UV dose is lost in the glass superstrate and/or interlayer adhesive, e.g., primer. For refractive optical systems, the use of a homogenizer has very little effect on UV dose relative to the material choice for the Fresnel lens (compare standard PMMA to standard PMMA//borosilicate homogenizer). The reflective optical systems are intermediate to standard PMMA and the most UV-transmitting lenses, including SOG, borosilicate glass, and UV-T PMMA. The greater UV reflectance of bare Al over bare Ag, Fig. 3 (left), would be expected to result in a greater UV dose for Al. In principle, an Al reflector would prove useful in an accelerated UV-aging fixture. In practice, the various layers used in representative reflector components may outweigh the significance of the base reflective layer, particularly for PMMA/Ag, which typically incorporates UV absorbers for enhanced stability and therefore reflects much less UV light (making it comparable to a standard PMMA lens). Although not shown in Fig. 6, the use of a borosilicate homogenizer in reflective optical systems will decrease the UV dose more significantly than in the refractive systems, i.e., attenuating 1/3 to 1/2 of the original UV dose. Although not shown in Table 6, the use of a quartz homogenizer would instead attenuate about 10% of the UV dose. The use of a front glass (compare Fig. 6 and Table 6 to Ref. 12) further reduces the UV dose by ~7–16%. The reduction is typically more significant for Al-based reflectors (~15% loss), where a greater amount of UV radiation is transmitted than Ag-based reflectors (~8% loss). In comparison, ~5% of the blue, red, and IR wavelengths are lost in the reflective systems by the incorporation of the soda-lime front glass. This throughput loss for the front glass could be reduced by at least 50% if both sides of the glass were AR-coated, Table 2.

Studies have suggested that tracking of the sun in two-axis trackers harnessing the direct and circumsolar radiation is required for $C_g > 2.1$ (Ref. 49), 5.2 (Ref. 50), or 15.6 (Ref. 51), respectively. The dependence of CPV on direct light may be its most significant limiting factor. Direct UV radiation is readily subject to scattering by moisture as well as the local atmospheric aerosol content; however, the arid and/or high-elevation locations most suited to CPV are known to have higher direct UV radiation.[52] A significant seasonal variation can also exist outside of tropical latitudes. For example, while the remainder of the solar spectrum may vary by about 3%, UV-A may vary by a factor of 1.6, and the most damaging UV-B may vary by 4× between solstices.[52] The location- and temporal-specific conditions combined with the dose factor suggested in Table 6 are therefore expected to increase the variability in photodegradation and resulting service life for CPV relative to FP-PV.

The increasing ability of photons to cause damage as their energy is increased (i.e., wavelength decreased) is inherently captured in Eq. (1). The action spectrum, which may vary in a complex manner with wavelength, is approximated in Eq. (1), as it has not been empirically determined for any of the encapsulation materials examined here. The action spectrum and coefficients considered, however, are most appropriate for hydrocarbons, where covalent carbon bonds in the backbone and/or side-groups of the polymer molecules become prone to scission for $\lambda \leq 360$ nm, i.e., bond dissociation energy of 83 kcal/mol for C–C.[53] In contrast, the covalent silicon bonds present in silicones, such as PDMS, become increasingly subject to scission for $\lambda \leq 250$ nm, i.e., bond dissociation energy of 108 kcal/mol for Si–O.[53] Figure 6 and Table 6 are therefore readily applicable to the hydrocarbon materials, but not necessarily the silicones.

4.2.2 *The unused IR radiation*

The UNIR energy flux density is also summarized in Table 6. Here, Eqs. (4) and (10) are applied for $\lambda = 1800$–2500 nm. As with the other wavelength regions, the FP-PV application is used in Table 6 as the reference for UNIR flux. Some results in the UNIR wavelengths are markedly different from those for UV. The Xe lamp emulates the solar UV and visible spectrum but generates no irradiation above $\lambda = 1300$ nm. Another distinct difference is the greater transmittance of all refractive optical systems in the UNIR range (where ϕ is ≥20% of the 500× concentrated flux) relative to the UV range (where ϕ can be ~1% of the concentrated flux). Because of the absorptance peaks for PMMA (Fig. 5), the glass lens transmits more UNIR than PMMA. For a SOG lens, the lesser thickness of the PDMS lens facets minimizes optical absorptance, rendering a stronger UNIR transmittance than PMMA. For the refractors, there is a ~27% or ~2% UNIR transmittance loss when a borosilicate or quartz homogenizer is used, respectively. The difference between the two materials comes from the decreasing transmittance of borosilicate glass above $\lambda = 2000$ nm, where the solar flux is limited in that wavelength region. From Table 2, however, the IR flux not utilized in MJ cells constitutes a small amount of energy. [An important distinction is that the UNIR wavelengths must first pass through the encapsulation (where ϕ_T is more similar to Ref. 12) before it is reflected back by the cell (the ϕ_T defined in Table 6)]. The absorption in the encapsulation occurring during the first optical pass is material specific (Fig. 5), and therefore has been generalized to the UNIR wavelengths here. In contrast, there is much less distinction between the reflective optical systems; all provide greater UNIR flux ($\phi \geq 44\%$ C_g, with several ≥84% C_g). The differences between the reflector components can arise from the particular layers used in their construction. An ~43 or ~6% loss, respectively, occurs when a borosilicate or quartz homogenizer is used with the reflectors. Importantly, when significant heating of the homogenizer occurs, it may contribute to heating the cell and its encapsulation. One unique instance is the use of a standard PMMA Fresnel lens combined with an anodized Al reflective homogenizer (the homogenizer is shielded from mechanical damage by being located inside the module). Here, there is a sizeable

reduction in both the UV and UNIR flux. Separately, the use of a front glass in the reflective systems results in a 6% loss in UNIR ϕ_T.

Regarding the flux related to energy production, φ_T and the related Effective C_g in Table 6 identify that the optical efficiency of the various CPV systems approaches 80–85% at best. The Effective C_g approaches 70% for the standard PMMA lens//borosilicate homogenizer, Anodized Al//borosilicate homogenizer, Standard PMMA//anodized Al homogenizer, and thin-glass/Ag//thin-glass/Ag//borosilicate homogenizer systems, i.e., the systems presently most commonly used with MJ cells. Of the wavelength bands associated with junctions in III-V cells, the Effective C_g is typically lesser for the blue junction, implying it is more likely to render a current-limiting condition. Because of the reduced reflectance of the Al base layer at $\lambda = 775$ nm, the red junction is instead most immediately likely to be current-limiting for the systems including ///Anodized Al/borosilicate homogenizer, ///Anodized Al, and ///Al reflector systems (all Al-enabled reflectors).

Table 6 identifies the increased significance of UNIR (as opposed to UV) exposure for CPV systems, particularly when the energy flux and corresponding cumulative thermal load becomes significant in concentrating modules, e.g., $C_g \geq \sim 50$. For some configurations, the UV dose may not greatly exceed the unconcentrated global solar condition, but the thermal load scales nearly directly with C_g. The reflectors examined in Fig. 3 and Table 4 come from the concentrating solar power (CSP) industry, where reflectance of IR flux is vital to the application. That is, the reflectors have not been tailored to the CPV application, where rejection of UNIR flux is desirable. Approaches that may be used to reduce the thermal flux include: (1) choosing an encapsulant exhibiting little direct absorptance of the solar spectrum, such as PDMS in Table 5, (2) choosing materials for optical components that maximize UNIR absorptance, such as a standard PMMA lens in Table 1 or an anodized Al reflector in Table 4. Here, incoming UNIR is absorbed up front at lesser concentration, before it reaches the vicinity of the cell. (3) Water is an excellent example of a liquid that absorbs the solar spectrum selectively for $\lambda > 1300$ nm.[17] The absorptance spectrum of water is ideally compatible with crystalline Si; if water could be incorporated into the first component(s) of the optical system, its reflective loss could be tolerated ($n \sim 1.33$), and freezing is not an issue. (4) The UNIR flux might be separated and/or defocused in the optical design of refractive components. (5) The thermal load may also be lessened by using thin film coating(s) as a "hot" heat mirror (reflecting or absorbing incoming UNIR, which may also increase power production[11,55]). (6) AR coating(s) present on the cell may reject UNIR flux below the bandgap (Table 2). (7) The use of a liquid such as silicone oil to fill the module cavity, improving thermal conductivity, might prove requisite in extreme situations. While the aforementioned techniques may prove beneficial, the most fundamental tactic to promote performance and reliability is a good system design that optimizes thermal management. Because most degradation processes (including photodegradation and hydrolytic degradation) are synergistically enhanced with temperature, good thermal management should improve reliability and promote long field life while enhancing on-sun cell efficiency.

A key assumption in the analysis (Fig. 6 and Table 6) is that the optical flux within each CPV system is uniform. The flux uniformity could easily vary by one to three orders of magnitude for a Fresnel lens, particularly when an imaging lens design is used without a homogenizer.[36] Likewise, mechanical damage such as retained deformation at impact sites on a mirror component could locally defocus light, creating localized variation in intensity. Temporal factors such as mechanically induced sag (snow, wind, or gravity), heterogeneous material degradation, moisture condensation, soiling, corrosion, abrasion, or degradation at interfaces may have a similar effect. The concern of flux uniformity is of increased importance for encapsulation used in CPV, where intense UV could prematurely motivate photodegradation or an IR hotspot could motivate thermal decomposition. A major difficulty is that sufficiently degraded regions of polymer are often more optically absorbing than unaffected material, motivating thermal runaway and subsequent risk of ignition.

4.3 *The Optical Reflectance and Electroluminescence of the PV Cell*

The final optical component in the system is the PV cell, which may reflect photons with energies below the bandgap. No cell technology provides perfectly efficient optical conversion; the flux reflected back through the encapsulation is therefore summarized in Table 7. Reflectance measurements were obtained for unpackaged cell specimens obtained from different vendors. Note that c-Si specimen #4 is CPV specific (i.e., having a greater gridline density), whereas the III-V specimens consist of the present $GaInP_2$/GaAs/Ge triple-junction technology.[1,54] The literature related to AR coatings provides representative (optimum) reflectance profiles for c-Si (Refs. 28 and 56) and MJ (Refs. 11 and 55) technology. The reflectance versus wavelength profiles (not shown) clearly evidence AR coatings for all of the cells in Table 7. In Table 7, a greater φ_R occurs for the CPV-specific c-Si cell, presumably because of enhanced reflection from gridlines. Greater φ_R occurs for the MJ technology in the IR wavelengths (ordinarily not current-limiting). The UV ϕ_R comprises the least energy of the wavelength regions distinguished in Table 7; the energy flux from 280–400 nm is similar for both c-Si and MJ technologies. The UNIR ϕ_R is greater for c-Si than MJ technology; however, in both technologies ϕ_R is a similar percentage of the overall IR flux.

The reflected flux in Table 7 is not immediately significant, but it will scale with the C_g of the optical system. Of the specimens in Table 7, the greatest reflectance is expected for the c-Si #4. Although the sub-component packaging (such as a coverglass) is present on the MJ specimens in Table 7, no additional packaging components are present on the bare c-Si cells examined. The light reflected from c-Si cells, however, tends to be scattered by texture, etched into the surface of the cell to promote absorption via reflection within Si. Reflectance at the cell is also subject to the backside metallization.[27] Above all, roughly equal percentages of UV and UNIR flux are reflected back to the encapsulant by the cell. After all, additional aging can be invoked by UV and UNIR flux transmitted through the encapsulant, when it is reflected back by the cell.

In addition to reflectance, electroluminescence occurring at the cell should also be considered. Because cells may radiate via electroluminescence at the bandgap in the open-circuit condition, the specimens in Table 7 were externally

Table 7 The (absolute) reflectance for c-Si and MJ cells; results are shown for multiple manufacturers.

	Blue, 300–650 nm		300–1120 nm or Red 650–890 nm		Infrared, 890–1800 nm		UV, 280–400 nm		UNIR, 1120–2500 or 1800–2500 nm	
Item	φ_R {A·m^{-2}}	φ_R {%}	φ_R {A·m^{-2}}	φ_R {%}	φ_R {A·m^{-2}}	φ_R {%}	ϕ_T {W·m^{-2}}	ϕ_T {%}	ϕ_T {W·m^{-2}}	ϕ_T {%}
c-Si (1)	N/A	N/A	19	3	N/A	N/A	6	17	57	32
c-Si (2)	N/A	N/A	27	4	N/A	N/A	4	12	24	14
c-Si (3)	N/A	N/A	37	6	N/A	N/A	6	18	31	18
c-Si (4)	N/A	N/A	73	12	N/A	N/A	7	21	41	23
Direct solar (c-Si)	N/A	N/A	594.9	100	N/A	N/A	34.7	100	175.5	100
Global solar (c-Si)	N/A	N/A	661.6	111	N/A	N/A	51.9	149	181.3	103
MJ (1)	8	4	12	5	45	11	3	10	6	18
MJ (2)	14	7	16	7	45	11	5	14	5	14
Direct solar (MJ)	213.0	117	223.5	109	402.7	105	32.0	149	32.3	100
Global solar (MJ)	249.7	100	243.8	100	421.3	100	51.9	100	32.6	101

shunted with a wire during the reflectance measurements. To explain, a lesser extent of electroluminescence will occur during the shunted or operating conditions, where it can be solely facilitated by photon recycling.[27,57] The MJ cells here will emit at 668 (for GaInP) and 885 (GaAs) nm as well as 1850 (Ge) nm in the open circuit condition. The former peaks do not overlap with the absorptance spectrum of the encapsulation materials (Fig. 5). The emission at 1850 may be absorbed in the encapsulation (Fig. 5). Emission for Ge, however, is like that for Si at 1050 nm (also considered to be an indirect bandgap), being both less intense and more broadly distributed about the bandgap.

4.3.1 *Future work, including temporal issues*

This study provides preliminary insight related to the performance of CPV systems and reliability of CPV encapsulation materials. Future research will include real-time field exposure to compare candidate encapsulant materials and identify failure modes. This work will involve the verification of the UV flux and operating temperature in CPV systems deployed in the field as well as indoor accelerated aging systems. The results will provide feedback concerning the relative importance of damaging UV and IR radiation.

Study of the performance and lifetime of contemporary PMMA formulations and Fresnel lens components will provide understanding of how the analysis here applies over time for refractive optical systems; separate study of reflector components is presently ongoing. Known degradation mechanisms include: the optical durability of PMMA (loss of transmittance with aging);[3] microcrazing and hazing of PMMA; fracture and mechanical fatigue of PMMA (e.g., associated with an impact event);[58,59] physical aging/shape change/warping of PMMA;[60] solid erosion of PMMA (wear due to sand impact or physical cleaning);[3,61,62] delamination of PDMS from the glass superstrate in SOG lenses;[63] change in focus of SOG lenses due to thermal misfit between components;[64] solarization of glass (a change in the transmitted spectrum associated with a change in the oxidation state of Fe);[65,66] delamination of component layers;[13] corrosion of reflective layers;[13] corrosion of glass (facilitated by the leaching of alkali species);[67,68] and soiling (reduced transmittance caused by accumulation of particulate matter).[3]

5 Conclusions

Using representative components, the wavelength-specific optical performance of CPV systems has been studied to identify implications on performance and reliability. Key results include the following:

CPV designs using PMMA deliver a relatively small dose (∼1%) of UV near the cell, whereas those using a SOG composite lens or reflective components deliver a much greater UV dose (in some cases nearly 50%). Acceleration of UV exposure relative to PMMA designs can be easily accomplished using UV-transmissive optics or an aluminum reflector, but acceleration relative to the reflective CPV designs requires an increase in optical concentration and/or an increase in temperature. In all cases, operation at increased temperature is anticipated to affect the reliability of CPV encapsulants.

For refractive optical components, the UV and IR transmittance for standard PMMA is much less (80% and 20%, respectively) than that of SOG or glass lenses. Regarding reflective optical components, Ag exceeds Al, except in the UV bands. The various reflector components differ depending on the particular layers used, e.g., the superstrate or adhesive layers. A PMMA superstrate reflects significantly less (23%) UV flux than glass or metal constructed reflectors. All reflectors (Al and Ag) provided equivalent IR reflectance. The use of a (soda-lime) front glass reduces the UV flux more (8–15%) than the junction specific and UNIR wavelengths (8–9%). Regarding candidate encapsulation materials, silicone was exceptionally transmitting, whereas ionomer, PVB, and TPU absorbed the most UV and UNIR light. All encapsulants examined here are highly transmitting, therefore factors

other than optical transmittance, including thermal management, durability, service life, and cost, may motivate their use. Regarding the junction-specific wavelengths, the majority of refractors and reflectors as well as the absorptance of the encapsulation materials favors a current-limiting condition for the blue junction (the exception being Al-enabled reflectors, which favor the red junction).

In the case of CPV (versus conventional flat-panel photovoltaics), thermal management is identified as of increased significance relative to UV radiation. The flux of unused IR light, however, is substantially (80%) less in MJ cell technology relative to crystalline silicon cells. The UNIR flux density typically scales more closely with the geometric concentration of solar radiation, whereas the UV flux may be substantially less than the nominal geometric concentration. In systems with low geometric concentration, where a single reflection may be used to concentrate light, the UV dose may well exceed that in systems with high geometric concentration, such as those utilizing a PMMA refractive optic with a secondary homogenizer. The analysis here, however, does not eliminate the importance of UV radiation; the findings do, however, suggest that thermal and/or related synergistic mechanisms, including photothermal and hydrothermal, will bear increased significance.

Regarding future material selection, module durability, qualification, and safety tests, the control of specimen temperature is highly important. The specific test conditions appropriate to CPV are yet to be determined; the conditions present in CPV modules may vary considerably according to the system design. The aging of optical components alters the activation spectrum (often the blue wavelengths), further complicating the findings of the study here. By leveraging existing optical durability studies of reflector components and examining the durability of refractive components, temporal issues affecting the reliability of encapsulation materials may be understood.

Acknowledgments

The authors are grateful to Dr. Keith Emery, Dr. Daryl Myers, Dr. John Pern, Matt Beach, Christa Loux, Marc Oddo, Bryan Price, Kent Terwilliger, and Robert Tirawat of the National Renewable Energy Laboratory for their discussion/help with the solar spectrum, experimental methods, and optical measurements, respectively; Dr. Margaret Fraelich of Fresnel Technologies Inc., Dr. Jayesh Bokria, Dr. Ryan Tucker, and Mr. Christopher Hastings of Specialized Technology Resources Inc., Roger French and Eric Romano of E.I. du Pont de Nemours and Co., Dr. Uwe Keller of Kuraray Europe GmbH, and Michelle Velderrain of NuSil Technology LLC for their help with specimen materials. As published data was previously unavailable for several materials, Roger French is gratefully acknowledged for facilitating refractive index measurements. This work was supported by the U.S. Department of Energy under Contract No. DE-AC36-08GO28308 with the National Renewable Energy Laboratory.

References

1. R. R. King, A. Boca, W. Hong, X.-Q. Liu, D. Bhusari, D. Larrabee, K. M. Edmondson, D. C. Law, C. M. Fetzer, S. Mesropian, and N. H. Karam, "Band-gap-engineered architectures for high-efficiency multijunction concentrator solar cells," *Proc. European Photovoltaic Solar Energy Conference (PVSEC)*, 24th conference,, 55–61 (2009).
2. M. A. Dunlap, W. Marion, and S. M. Wilcox, "Solar radiation data manual for flat-plate and concentrating collectors," *NREL/TP* **463-5607**, 1–259 (1994).
3. D. C. Miller and S. R. Kurtz, "The durability of fresnel lenses: a review specific to the concentrating photovoltaic application," *in preparation*.
4. "IEC 62108 Concentrator Photovoltaic (CPV) Modules and Assemblies – Design Qualification and Type Approval," International Electrotechnical Commision: Geneva, 1–84 (2007).
5. J. W. Martin, J. A. Lechner, and R. N. Varner, "Quantitative characterization of photodegradation effects of polymeric materials exposed in weathering environments," *ASTM Spec. Tech. Publ.* **1202**, 27–51 (1994).
6. A. L. Andrady, "Wavelength sensitivity in polymer degradation," *Adv. Polym. Sci.* **128**, 47–94 (1996).
7. M. D. Kempe, M. Kilkenny, and T. J. Moricone, "Accelerated stress testing of hydrocarbon based encapsulants for medium-concentration CPV applications," *Proc. IEEE PVSC*, 001826–001831 (2009).
8. A. L. Andrady, S. H. Hamid, X. Hu, and A. Torikai, "Effects of increased solar ultraviolet radiation on materials," *J. Photochem. Photobio. B* **46**, 96–103 (1998).
9. N. D. Searle, "Activation spectra: Techniques and applications to stabilization and stability," *ASTM Spec. Tech. Publ.* **1202**, 41–58 (1994).
10. G. Kämpf, K. Sommer, and E. Zirngiebl, "Studies in accelerated weathering. Part I. determination of the activation spectrum of photodegradation in polymers," *Prog. Org. Coat.* **19**, 69–77 (1991).
11. H. Yoon, D. E. Joslin, D. C. Law, D. Krut, R. R. King, P. Vijayakumar, D. Peterson, J. Hanley, and N. Karam, "Application of infrared reflecting (IRR) coverglass on multijunction III-V solar cells," *Proc. WCPEC the "World Conference on Photovoltaic Energy Conversion"*, 4th conference, 1861–1864 (2006).
12. D. C. Miller, M. D. Kempe, C. E. Kennedy, and S. R. Kurtz, "Analysis of transmitted optical spectrum enabling accelerated testing of CPV designs," *Proc. SPIE* **7407**, 7407–7416 (2009).
13. C. E. Kennedy and K. Terwilliger, "Optical durability of candidate solar reflectors." *Journal of Solar Energy Engineering, Transactions of the ASME* **127**, 262–269 (2005).
14. "*ASTM E903* standard test method for solar absorptance, reflectance, and transmittance of materials using a integrating sphere," ASTM International, West Conshohocken, 1–9 (1996).
15. "*ASTM G173* standard tables for reference solar spectral irradiances," ASTM International, West Conshohocken, 1–20 (2003).
16. "*ASTM G177* standard tables for reference solar ultraviolet spectral distributions: hemispherical on 37° tilted surface," ASTM International, West Conshohocken, 1–9 (2003).
17. E. D. Palik, *Handbook of Optical Constants of Solids*, Academic Press Limited, London (1998).
18. E. Lorenzo and G. Sala, "Hybrid silicone-glass Fresnel; lens as concentrator for photovoltaic applications," *Proc. Int. Solar Energy Soc (Vol. 1): Silver Jubilee Congress, Atlanta, Pergamon Press*, 536–539 (1979).
19. J. S. Stroud, "Photoionization of Ce3 + in glass," *J. Chem. Phys.* **35**(3), 844–850 (1961).
20. S. B. Donald, A. M. Swink, and H. D. Schreiber, "High-iron ferric glass," *J. Non-Cryst. Sol.* **352**, 539–543, (2006).
21. A. N. Cox, Ed., *Allen's Astrophysical Quantities*: 4th Edition, Springer, New York (1999).
22. G. Rottman, "Solar ultraviolet irradiance and its temporal variation," *J. Atmos. Sol. Terr. Phys.* **61**, 37–44 (1999).
23. L. S. Rothman, I. E. Gordona, A. Barbe, D. Chris Benner, P. F. Bernath, M. Birk, V. Boudon, L. R. Brown, A. Campargue, J.-P. Champion et al., "The HITRAN 2008 molecular spectroscopic database," *J. Quant. Spectrosc. Radiat. Transf.* **110**(9-10), 533–572 (2009).
24. A. L. Andrady, "Wavelength sensitivity in polymer photodegradation," *Adv. Polym. Sci.* **128**, 47–94 (1997).
25. A. L. Andrady, S. H. Hamid, X. Hu, and A. Torikai, "Effects of increased solar ultraviolet radiation on materials," *J. Photochem. Photobiol. B* **46**, 96–103 (1998).
26. N. D. Searle, "Activation spectra: techniques and applications to stabilization and stability," *ASTM Spec. Tech. Publ.* **1202**, 41–58 (1994).
27. J. F. Geiz, D. J. Friedman, S. R. Kurtz, M. A. Steiner, W. E. McMahon, L. Gedvilas, A. Duda, M. Young, and W. Olavarria, "Cell-level thermal management issues in concentrator III-V multijunction solar cells," *Proc. IEEE Photovoltaic Specilists Conference (PVSEC)*, 35th conference, (2010).
28. A. Gombert, W. Glaubitt, K. Rose, J. Driebholz, B. Blasi, A. Heinzel, D. Sporn, W. Döll, and V. Wittwer, "Antireflective transparent covers for solar devices," *Sol. Eng.* **68**, 357–360 (2000).
29. M. Chen, H.-C. Chuang, A. S. P. Chang, S.-Y. Lin, J.-Q. Xi, and E. F. Schubert, "Design of optical path for wide-angle gradient-index antireflection coatings," *Appl. Opt.* **46**(26), 6533–6538 (2007).
30. S. J. Wilson and M. C. Hutley, "The optical properties of 'moth eye' antireflection surfaces," *Opt. Acta.* **29**(7), 993–1009 (1982).
31. ZEMAX Optical Design Software, available from: http//www.focus-software.com., 1999.
32. R. H. French, J. M. Rodríquez-Parada, M. K. Yang, R. A. Derryberry, M. F. Lemon, M. J. Brown, C. R. Haeger, S. L. Samuels, E. C. Romano, and R. E. Richardson, "Optical properties of materials for concentrator

photovoltaic systems," *Proc. IEEE Photovoltaic Specilists Conference (PVSEC)*, 34th conference, 000394–000399 (2009).
33. Dow Corning Corp., "Develop silicone encapsulation systems for terrestrial silicon solar arrays," DOE/JPL-954995-80, 1–57 (1979).
34. Y. Israëli, J. Lacoste, J. Cavezzan, and J. Lemaire, "Photooxidation of polydimethylsiloxane oils and resins. IV–effect of phenyl groups," *Polym. Degrad. Stab.* **47**, 357–362 (1995).
35. G. Deshpande and M. E. Rezac, "The effect of phenyl content on the degradation of poly(dimethyl diphenyl) siloxane copolymers," *Polym. Degrad. Stab.* **74**, 363–370 (2001).
36. R. Leutz and A. Suzuki, *Nonimaging Fresnel-lenses: Design and Performance of Solar Concentrators*, Springer, New York (2001).
37. J. E. Greivenkamp, *Field Guide to Geometrical Optics*, SPIE Press, Bellingham (2004).
38. S. N. Kasarova, N. G. Sultanova, C. D. Ivanov, and I. D. Nikolov, "Analysis of dispersion of optical plastic materials," *Opt. Mater.* **29**, 1481–1490 (2007).
39. M. Rubin, "Optical properties of soda lime glasses," *Solar Energy Materials* **12**, 275–288 (1985).
40. D. C. Miller, L. M. Gedvilas, B. To, C. E. Kennedy, and S. R. Kurtz, "Durability of poly(methyl methacrylate) lenses used in concentrating photovoltaics," *Proc. SPIE.* **7773**, 7773–2 (2010).
41. K. R. McIntosh, J. N. Cotsell, J. S. Cumpston, A. W. Norris, N. E. Powell, and B. M. Ketola, "An optical comparison of silicone and EVA encapsulants for conventional silicon PV modules: a ray-Tracing study," *Proc. IEEE Photovoltaic Specilists Conference (PVSEC)*, 34th conference, 544–549 (2009).
42. J. Kapur, K. Proost, and C. A. Smith, "Determination of moisture ingress through various encapsulants in glass/glass laminates," *Proc. IEEE Photovoltaic Specilaists Conference (PVSEC),*, 34th conference, 001210–001214 (2009).
43. T. Swonke and R. Auer, "Impact of moisture on PV module encapsulants," *Proc. SPIE* **7412**, 74120A (2009).
44. D. Kockott, "Factors influencing the reliability of results in accelerated weathering tests," *ASTM Spec. Tech. Publ.* **1294**, 24–39 (1996).
45. A. W. Czanderna and F. J. Pern, "Encapsulation of PV modules using ethylene vinyl acetate copolymer as a pottant: a critical review," *Solar Energy Materials and Solar cells*, **43**, 101–181 (1996).
46. P. Klemchuck, M. Ezrin, G. Lavigne, W. Holley, J. Galica, and S. Agro, "Investigation of the degradation and stabilization of EVA-based encapsulant in field-aged solar energy modules," *Polymer Degradation and Stability*, **55**, 347–365 (1997).
47. N. S. Allen, M. Edge, M. Rodriguez, C. M. Liauw, and E. Fontan, "Aspects of the thermal oxidation, yellowing and stabilization of ethylene vinyl acetate copolymer," *Polymer Degradation and Stability*, **71**, 1–14 (2001).
48. M. D. Kempe, G. J. Jorgensen, K. M. Terwilliger, T. J. McMahon, C. E. Kennedy, and T. T. Borek, "Acetic acid production and glass transition concerns with ethylene-vinyl acetate used in photovoltaic devices," *Solar Energy Materials and Solar cells*, **91**, 315–329 (2007).
49. M. Collares-Pereria, "High temperature solar collector with optimal concentration: nonfocusing Fresnel lens with secondary concentrator," *Sol. Eng.* **23**, 409–420 (1979).
50. R. Winston and W. Zhang, "Pushing concentration of stationary solar concentrators to the limit," *Opt. Exprss* **18**, A64–A72, (2010).
51. R. Leutz, A. Suzuki, A. Akisawa, and T. Kashiwagi, "Design of a nonimaging fresnel-lens for solar concentrators," *Sol. Eng.* **65**(6), 379–387 (1999).
52. G. A. Zerlaut, "Solar ultraviolet radiation: aspects of importance to the weathering of materials," *Accelerated and Outdoor Durability Testing of Organic Materials, ASTM Spec. Tech. publ.* **1202**, 3–26 (1994).
53. M. D. Kempe, "Evaluation of encapsulant materials for PV applications," submitted to *Photon International*.
54. A. Luque and S. Hegedus, *Handbook of Photovoltaic Science and Engineering*, Wiley, Hoboken, NJ (2003).
55. R. Moy, "Solar Power Collection with Near Infrared Wideband Reflector Coating" U.S. Patent No. US2005/0103374A1 (May 19, 2005).
56. H. M. Branz, V. E. Yost, S. Ward, K. M. Jones, B. To, and P. Stradins, "Nanostructured black silicon and the optical reflectance of graded-density surfaces," *Appl. Phys. Lett.* **94**, 231121 (2009).
57. S. Kurtz, D. Meyers, W. E. McMahon, J. Geisz, and M. Steiner, "A comparison of theoretical efficiencies of multi-junction concentrator solar cells," *Progress in Photovoltaics: Research and Applications* **16**, 537–546 (2008).
58. V. T. Truong, P. E. M. Allen, and D. R. G. Williams, "The effect of molecular-properties on mechanical-behavior of poly(methyl methacrylate): 1. Stress cracking in air," *Euro. Polymer J.* **22**, 903–910 (1986).
59. T. R. Clark, R. W. Hertzberg, and N. Mohammadi, "Fatigue mechanisms in poly(methyl-methacrylate) at threshold-effects of molecular-weight and mean stress," *J. Mater. Sci.* **28**, 5161–5168 (1993).
60. R. Greiner and F. R. Schwarzl, "Thermal contraction and volume relaxation of amorphous polymers," *Rheol. Acta* **23**, 378–395 (1984).
61. H. Hojo, K. Tsuda, and C. M. Thai, "Erosion damage of polymethyl methacrylate," *Zairyo/Journal of the Society of Materials Science* **29**, 731–735 (1980).
62. H. Getu, A. Ghobeity, J. K. Spelt, and M. Papini, "Abrasive jet micromachining of polymethylmethacrylate," *Wear* **263**, 1008–1015 (2007).
63. R. Leutz, L. Fu, and H. P. Annen, "Stress in large-area optics for solar concentrators," *Proc. SPIE* **7412**, 741206 (2009).
64. T. Hornung, A. Bachmaier, P. Nitz, and A. Gombert, "Temperature dependent measurement and simulation of fresnel lenses for concentrating photovoltaics," Intl. Conf. CPV Systems, 2010.
65. J. Vitko and J. E. Shelby, "Solarization of heliostat glasses," *Sol. Energy Mater.* **3**, 69–80 (1980).
66. A. J. Faber, "Optical properties and redox state of silicate glass melts," *C. R. Chim.* **5**, 705–712 (2002).
67. C. G. Pantano, D. E. Clark, and L. L. Hench, *Corrosion of Glass*, Books for Industry and the Glass Industry, New York (1979).
68. R. G. Newton, "The durability of glass — a review," *Glass Technol.* **26**, 21–38 (1985).

David C. Miller received the PhD degree in mechanical engineering from The University of Colorado at Boulder, in 2006. He has worked with microsystems including optical MEMS as well as characterization of nanomaterials in academic and industry settings. He now specializes in materials characterization for the purpose of durability assessment, reliability prediction, and standardization of photovoltaic (PV) modules. Current activities include: (a) the "optical side" of concentrating photovoltaics, including encapsulation materials as well as optical components (Fresnel lenses); (b) phase change and viscoelastic flow ("creep") in polymeric materials for conventional flat plate modules, including crystalline-Si and thin film technologies; (c) the durability of PV module components, including AR coatings, glass, and the junction-box.

Michael D. Kempe received the PhD degree in chemical engineering from California Institute of Technology in 2003. Since then, he has served as a scientist in the PV Module Reliability Group of the National Center for Photovoltaics at the National Renewable Energy Laboratory, where he studies the factors affecting the longevity of photovoltaic cells and modules. His work is primarily concerned with both modelling and measuring moisture ingress into PV modules and studying its effect on polymer adhesion, device performance, and component corrosion. He is also studying the effects of UV radiation on the stability of PV components.

Cheryl E. Kennedy specializes in the durability of advanced solar reflectors, absorbers, and transparent polymer films; development of advanced solar reflectors, high-temperature absorbers, and barrier coatings; thin-film physical vapor deposition. She is known for understanding performance and durability of optical materials, accelerated-testing equipment capabilities and applications; thin-film deposition of reflective and barrier coatings; 3- and 5-chamber deposition system capabilities and applications.

Sarah R. Kurtz obtained her PhD degree in chemical physics in 1985 from Harvard University and has worked since then at the National Renewable Energy Laboratory, in Golden, CO. She is best known for her contributions to developing multijunction, GaInP/GaAs solar cells and for supporting the Concentrator Photovoltaic (PV) industry. Currently, she is managing the Reliability Group at NREL and working to facilitate the growth of the PV industry, through improved performance of PV in the field.